

Enhanced Tunnelling in a Hybrid of Single-Walled Carbon Nanotubes and Graphene

Yongping Liao,^{†,||} Kimmo Mustonen,^{*,‡,||} Semir Tulic,[‡] Viera Skakalova,[‡] Sabbir
A. Khan,[¶] Patrik Laiho,[†] Qiang Zhang,[†] Changfeng Li,[§] Mohammad R.A.
Monazam,[‡] Jani Kotakoski,[‡] Harri Lipsanen,[§] and Esko I. Kauppinen^{*,†}

[†]*Aalto University School of Science, Department of Applied Physics, P.O. Box 15100,
FI-00076 Aalto, Finland*

[‡]*University of Vienna, Faculty of Physics, 1090 Vienna, Austria*

[¶]*Niels Bohr Institute, University of Copenhagen, 2100 Copenhagen, Denmark*

[§]*Nanoscience and Advanced Materials Group, Department of Micro- and Nanosciences,
Micronova, Aalto University, P.O. Box 13500, FI-00076 Aalto, Finland*

^{||}*Contributed equally to this work.*

E-mail: kimmo.mustonen@univie.ac.at; esko.kauppinen@aalto.fi

Abstract

Transparent and conductive films (TCFs) are of great technological importance. The high transmittance, electrical conductivity and mechanical strength make single-walled carbon nanotubes (SWCNTs) a good candidate for their raw material. Despite the ballistic transport in individual SWCNTs, however, the electrical conductivity of their networks is limited by low efficiency of charge tunneling between the tube elements. Here, we demonstrate that the nanotube network sheet resistance at high optical transmittance is decreased by more than 50% when fabricated on graphene and thus provides a comparable improvement as widely adopted gold chloride (AuCl₃)

doping. However, while Raman spectroscopy reveals substantial changes in spectral features of doped nanotubes, no similar effect is observed in presence of graphene. Instead, temperature dependent transport measurements indicate that graphene substrate reduces the tunneling barrier heights while its parallel conductivity contribution is almost negligible. Finally, we show that combining the graphene substrate and AuCl₃ doping, the SWCNT thin films can exhibit sheet resistance as low as 36 Ω/□ at 90% transmittance.

Keywords: SWCNT, graphene, transport, conductivity, transparent and conductive films

The electrical transport in networks of single-walled carbon nanotubes (SWCNTs) vary in a wide range of values as the structure of tubes and the morphology of networks differ. Since the modest conductivity reported in the seminal demonstrations,^{1,2} the performance has gradually improved through morphological optimization³⁻⁹ and progress in non-covalent doping.^{5,10-12} Meanwhile, as confirmed by numerous direct measurements,¹³⁻¹⁵ the limiting factor in network conductivity remains to be the inefficient charge tunneling between individual tubes and thus, the central paradigm lies in their interface optimization. In this role the contacts have been bridged for example by using suitable work function metals¹⁶ and also more recently, with graphitized carbon welds.⁹ The latter approach has proven particularly successful and the thin film performance (as measured by the ratio of conductance and absorbance) approaches the projected ultimate limit for SWCNT transparent electrodes.^{8,17} In the same spirit graphene and nanotubes have been combined into hybrid thin films,¹⁸⁻²⁷ although with performance not higher than that has been separately reported for pristine SWCNTs.^{4,5,7,28}

In this article, we present a detailed study of charge transport in SWCNT networks on a dielectric surface and on graphene; a division that has not been previously addressed in required detail. In contrast to most SWCNTs deposited through liquid phase, we have used a floating catalyst synthesis approach²⁹ that does not compromise the tube cleanliness

and quality by surfactant treatments. By using the same nanotube raw material, we have fabricated thin films on both a dielectric and a graphene substrate and have studied their charge transport and optical transmittance in pristine and doped states. On graphene, the SWCNT conductivity is found to be increased by a similar amount as is induced by chemical doping. Nevertheless, contrary to chemical doping, Raman spectroscopic measurements indicate no evidence of charge transfer between the nanotube and graphene layers. Instead, we establish the presence of graphene decreases the tunneling barrier heights and thus results in efficient inter-tube charge transport and hence greatly improved conductivity.

Results and Discussion

The SWCNT raw material was grown in a vertically assembled floating catalyst reactor (see Methods and Figure 1a).²⁹⁻³¹ With the same approach, some of us have earlier demonstrated that SWCNT properties can be tuned by small changes in the composition of synthesis atmosphere.³¹ In this work we used a composition that concurrently maximizes both the tube diameter and length, which according to earlier electron microscopy experiments correspond to 1.9 ± 0.5 nm and 7.5 ± 5.6 μm , respectively.²⁹ For optical and electrical characterization, the nanotube films were either accumulated directly on the target substrate by using a thermophoretic precipitator (TP)³² or, for reference purpose, by vacuum filtration and press-transfer (see Figure 1b-c).⁴

The sheet conductance (σ) and optical absorbance (A) of a uniform SWCNT film are directly related. This constant of proportionality can be understood as the quality factor (K) of the carbon nanotube raw material. Written using the Beer-Lambert law describing the attenuation of light in continuum media and sheet resistance (R_s) yields

$$K = \sigma \times A^{-1} = [R_s \times \log_{10}(T)]^{-1}, \tag{1}$$

where the latter equality is an alternative expression using optical transmittance (T). Thus, when the network's density is far above the percolation threshold,³³ R_s and T have a log-linear relation. The measured values for different SWCNT film thicknesses gathered for our experiments are shown in Figure 1e, and their R_s vary in a wide range from $\sim 170 \Omega/\square$ up to $\sim 3.5 \text{ k}\Omega/\square$. The trendlines visible in the plots are fitted according to Equation 1.

SWCNT films made by the two deposition techniques exhibit slightly different sheet resistance characteristics. At for example 90% transmittance the R_s of TP deposited (as estimated from the trendlines) equals to $\sim 450 \Omega/\square$, whereas the corresponding value for filtered networks is $\sim 330 \Omega/\square$. The sheet resistance scaling as a function of optical density (or films thickness) is also very different. At low density ($T \geq 92\%$), the TP deposited nanotubes

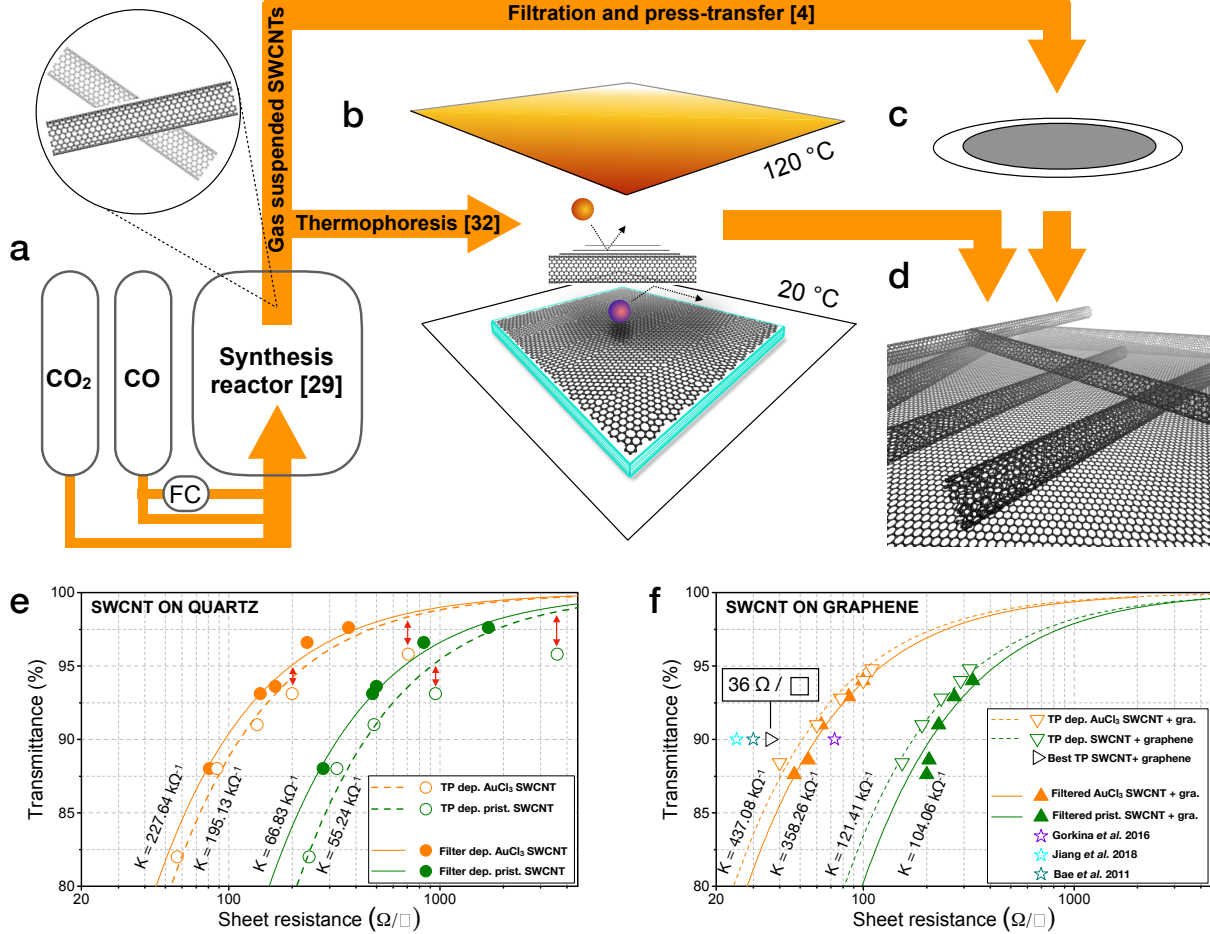


Figure 1: **TCF fabrication and the optoelectronic performance.** (a) A schematic of the floating catalyst synthesis reactor.^{29,30} FC, CO and CO₂ stand for the ferrocene cartridge, and carbon monoxide and dioxide gas cylinders. (b) A schematic depiction of direct SWCNT deposition using thermophoretic precipitator³² (TP) on graphene electrode and (c) on a membrane filter.⁴ (d) An artistic rendition of SWCNTs interfacing with graphene. (e) The sheet resistance vs. transmittance data for SWCNTs on quartz and (f) SWCNTs on graphene. The curves are fits to Equation 1.

show, reproducibly R_s that is higher than predicted by the bulk model in Equation 1 (see the highlighted data in Figure 1e). Such is, however, not the case for filtrated networks as is also corroborated by our earlier similar experiments.^{4,8,28} Since all TCFs were fabricated from virtually identical SWCNTs, these qualitative differences must emerge from the organization of the individual tubes and their interconnections, which we will discuss later. The addition of graphene layer in between the quartz substrate and the nanotube network decreased the R_s substantially (Figure 1f). The largest change was observed for TP deposited SWCNTs,

dropping from $\sim 450 \Omega/\square$ to $\sim 180 \Omega/\square$ and thus totalling 60%. This is particularly interesting, since the R_s of substrate-supported graphene is much higher, typically in the range of $700 \Omega/\square$ to $1000 \Omega/\square$. Meanwhile the decrease in filtered (and press-transferred) networks was a more moderate 35%, equalling a drop from $\sim 330 \Omega/\square$ to $\sim 215 \Omega/\square$.

The films were next treated with 16 mM gold chloride in acetonitrile solution (AuCl_3 , see Methods), further decreasing the R_s . The lowest R_s was achieved with the TP SWCNTs on graphene, yielding on average $\sim 50 \Omega/\square$ at 90% transparency. Also, the doping seems to improve the performance by the same factor regardless of the initial sheet resistance. Thus for example the filtered SWCNTs on graphene only reached $\sim 65 \Omega/\square$ but on quartz they still performed better than the TP SWCNTs ($\sim 95 \Omega/\square$ vs. $\sim 115 \Omega/\square$). The best TP deposited SWCNTs reached a value as low as $\sim 36 \Omega/\square$, which is among the lowest reported for any carbon based TCFs.^{9,19,34}

One could argue whether the observed improvement in presence of graphene is emerging from current distributing over the two parallel conduction layers (graphene and nanotubes). As intriguing as this idea is, it fails to provide even remotely correct predictions. Calculating for example the combined R_s using $\sim 750 \Omega/\square$ (the resistance of TP deposited SWCNTs at $T \sim 92.5\%$, Figure 1e) and an optimistic value of $\sim 650 \Omega/\square$ for graphene yields $\sim 350 \Omega/\square$. This result is roughly twice as high as the measured $\sim 180 \Omega/\square$. For filtered networks the discrepancies are clearly smaller (10-20%), indicating the layers are much less interconnected and are better described by the parallel approximation.

We next turned our attention to the mechanisms that could explain the observed improvement. From earlier contributions we know that charge tunneling efficiency between individual tubes can be visualized by temperature dependence of conductance. The mechanism is well understood within the framework of so called fluctuation-assisted tunneling (FAT) model,³⁵ often amended with an additional term describing the phonon backscatter-

ing.^{36,37} For sheet resistance it can be written as:

$$R(T) = A \times \exp\left(-\frac{T_m}{T}\right) + B \times \exp\left(\frac{T_b}{T_s + T}\right), \quad (2)$$

where the geometric factors A and B can be taken as constants. Here the first term reflects the backscattering by lattice vibrations with a characteristic phonon energy $k_B T_m$ (k_B being the Boltzmann constant) and the second term fluctuation-assisted tunneling through the energy barriers, $k_B T_b$, dividing the metallic regions. The parameter T_s is the tunneling efficiency near $T=0$ K where conductance reaches a value $(B \times \exp[T_b/T_s])^{-1}$.

Considering the anomalously low R_s was pronounced in the graphene-supported TP SWCNTs, we studied their transport in a liquid helium cryostat (Methods). The experimental results are presented in Figure 2, including pristine SWCNTs supported on SiO_2 (green curve), AuCl_3 -doped SWCNTs on SiO_2 (blue curve), graphene (orange curve), and SWCNTs on graphene (red curve). Generally the following is observed: **I.** The conductivity of the thin films containing nanotubes soar as a function of temperature until a maximum is reached, again decreasing at higher temperatures. **II.** The monolayer graphene's $G(T)$ curve (and thus the absolute conductivity) is an order of magnitude below the 90% transparency SWCNT films on SiO_2 . **III.** Placing SWCNTs on graphene and doping them with AuCl_3 has a similar impact on the conductivity. **IV.** The rate of decrease of $G(T)$ at high temperatures is steeper for SWCNTs on graphene than that of the doped nanotube films. Since in the cryostat instead of resistance we measured the sheet conductance, to fit the measurement results we also need to rewrite the FAT model as:

$$G(T) = G_0 + G_1 \times \left[\exp\left(-\frac{T_m}{T}\right) + \exp\left(\frac{T_b}{T_s + T}\right) \right]^{-1}, \quad (3)$$

where G_0 and G_1 are constants in the units of [S]. The parameters are listed in Table 1.

The exponentials in Equations 2 and 3 can be understood as a trade-off between the temperature-assisted charge tunneling through energy barriers that separate the metallic

Table 1: The parameters extracted by fitting Equation 3 to data in Figure 2.

	G_0, S	G_1, S	T_m, K	E_m, eV	T_b, K	T_s, K
Graphene	0.0002	0.0004	1078	0.093	2.10	14.85
SWCNTs	-0.0411	0.0549	970	0.084	5.36	20.72
SWCNTs + Graphene	-0.0196	0.0372	726	0.063	3.81	12.48
SWCNTs + AuCl ₃	-0.0104	0.0279	806	0.069	4.17	11.34

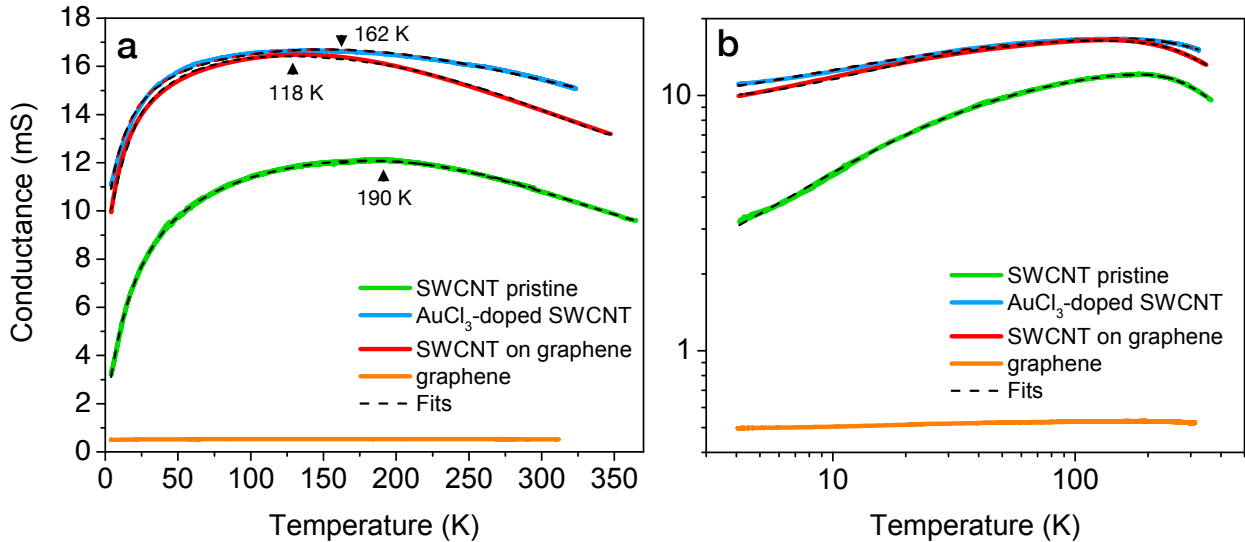


Figure 2: **Temperature dependent conductance.** The $G(T)$ plots for TP deposited SWCNTs on SiO₂ (green), on graphene (red), doped with AuCl₃ (blue) and for graphene (orange) with linear axis in (a) and in (b) log-log.

regions and the phonon scattering. The fitted values of T_m in our thin films span from 700 K to 1100 K (60-100 meV) and correspond to acoustic-phonons also visible as radial breathing modes (RBMs) in Raman spectra (see Figure 3b). The lowest value, $T_m=726$ K, was observed for SWCNTs on graphene and thus reflects the lowest phonon energy with the maximum of $G(T)$ at 118 K. Meanwhile the T_m for doped SWCNTs on SiO₂ was 806 K with $G(T)$ maximum at 162 K and for pristine SWCNTs 970 K with $G(T)$ maximum at 190 K. Thus the phonon energies are affected both by addition of a graphene layer and by chemical doping. The tunneling barrier heights corresponding to $k_B T_b$ are also affected, being $\sim 29\%$ lower for SWCNTs on graphene than on SiO₂ (see T_b in Table 1). A very similar effect, however, was also observed upon chemical doping, evoking a question whether graphene also possibly acts on SWCNTs as a dopant.

This possibility can be quickly ruled out by Raman spectroscopic measurements with a G-band mode ($\sim 1580 \text{ cm}^{-1}$) blue-shift expected upon both donor or acceptor doping. No such shift, however, could be detected upon deposition on graphene (Figures 3a-b). We did, however, observe a tiny broadening of the RBMs, which could indicate stronger van der Waals (vdW) interaction with the graphene substrate. Meanwhile, the spectrum of AuCl_3 doped SWCNTs (with a similar effect on the conductivity, see Figure 2) was clearly shifted by 4 cm^{-1} and the RBMs appear to be completely changed due to a change in resonant conditions. Looking at the optical absorption spectra (OAS, Figure 3c) we observe a minor suppression of the first semiconducting transition peak (S_{11}) on graphene. While this could indicate a mild charge transfer, it is certainly not comparable to suppression of all transitions (metallic and semiconducting) upon chemical doping. Although the transition peaks are unquestionably broader on graphene, this can be attributed to perturbations in the exciton lifetime resulting from dielectric screening³⁸ and thus supports the postulation of stronger vdW interaction in presence of graphene.

Interfacing of SWCNTs and graphene can be studied using atomically resolved scanning transmission electron microscopy (STEM, see Methods).³⁹ We first exposed the sample surfaces for observations by applying laser cleaning in the microscope column,⁴⁰ using a 10 ms pulse length with a total energy of 60 mJ. Our earlier observations revealed that when the thermodynamic constraints allow, thermophoretically deposited nanotubes form hundreds of nanometers long preferentially stacked interfaces with graphene. Our observations here suggest that regardless of higher rigidity of nanotube bundles,⁴¹ similar to individual tubes, they become completely in contact with the underlying graphene substrate. Figure 4a shows an example field of view acquired by medium-angle annular dark-field detector (MAADF) with several bundles crossing on graphene, all sharing the common focus and thus, the z-height.³⁹ This is even more evident in the atomically resolved closeups shown in Figure 4b and Supplementary Figure S1. Now, assuming that a minor alignment of interfaces is also possible at room temperature during the nanotube deposition³⁹ and noting that the mea-

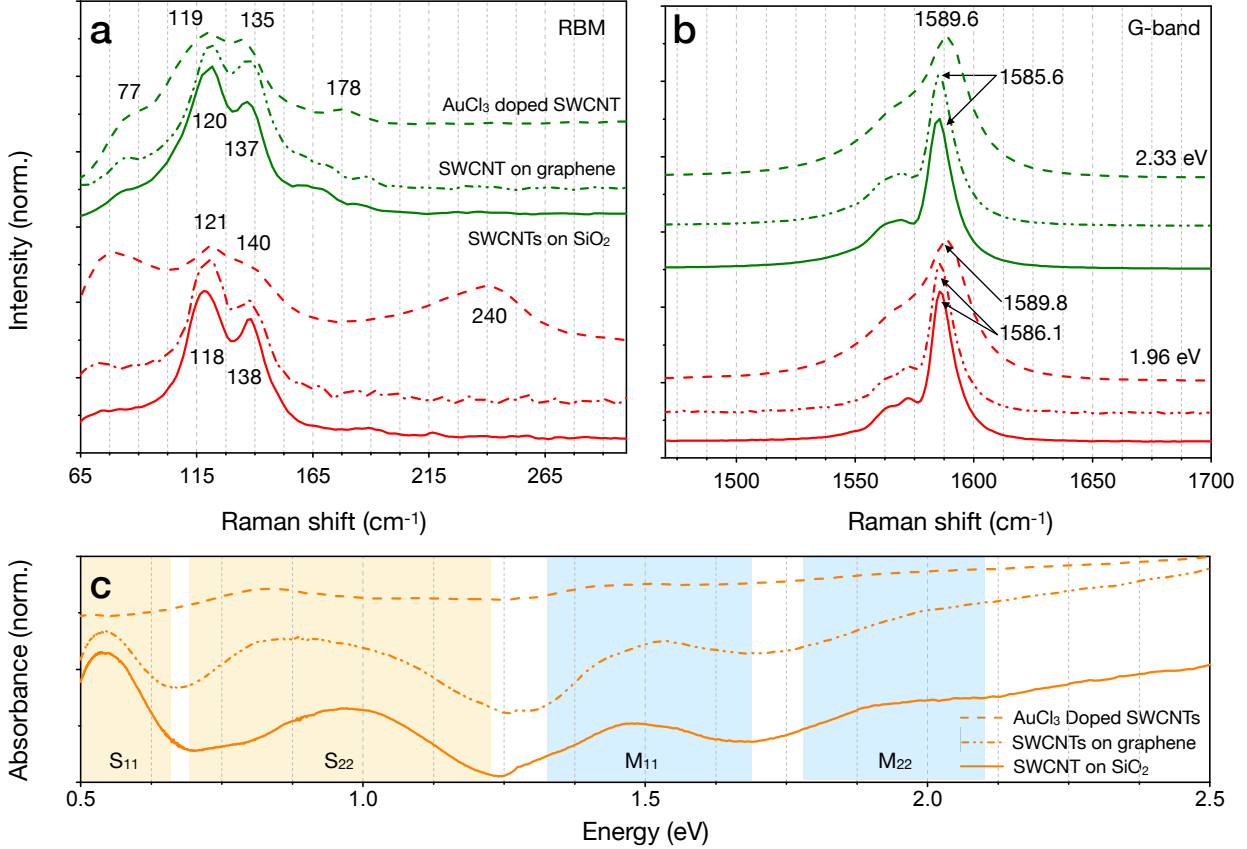


Figure 3: **Spectroscopic characterization.** (a) Raman radial breathing modes of SWCNT networks on graphene, on SiO₂ and those treated with AuCl₃, and (b) the corresponding G-band modes (2.33 and 1.96 eV laser lines). (c) The optical absorption spectra (OAS) measured on quartz. All samples were deposited using TP.

measurements conducted by Paulson *et al.* show that this considerably improves the charge transport through the interface,⁴² the conductivity could also drastically improve. Indeed, if we now turn our attention to the scanning electron microscopy (SEM, see Methods) images acquired from the nanotube samples on graphene and SiO₂ in Figures 4c-d, we observe a clear difference in their apparent contrast. As pointed out by the earlier authors,^{43,44} this kind of effect can well emerge when nanotubes are poorly interconnected, as for example when disconnected from their neighbours on a dielectric surface.

Finally, Sun *et al.* concluded that the transconductance of SWCNT is sensitive to the inter-tube contact morphology.⁴⁵ Their observation was that so called tube-tube Y-junctions, which our elongated graphene/SWCNT interfaces superficially resemble, were

generally more conductive than simple point contacts (X-junctions). This could explain the low barriers and low R_s of TP deposited SWCNTs on graphene, as they appear to be well interconnected with and through the graphene substrate. Further on, this can also explain why TP deposited SWCNTs on quartz exhibited an anomalously high R_s at low densities. As evident from for example Figure S2a, a low density TP deposited film is completely dominated by X-junctions and would thus be poorly interconnected without the presence of graphene. In contrast, Sun *et al.* observed networks with a very similar density fabricated by filter transfer, yet they had mainly Y-junctions in their experiments.⁴⁵ Although they did not specifically study the mechanism of junction formation, we believe that the prominence of Y-junctions can emerge in the presence of surface roughness of the filter, providing a greater degree of freedom for the nanotubes to mutually align. In the same manner, the Y-junctions also appear in thicker TP samples (Figure S2b), indicating that the surface roughness does indeed play an important role in the formation of Y-junctions.

Conclusions

To summarize, we have studied the mechanism of charge transport in SWCNT networks on graphene and on a dielectric substrate in their pristine and doped state. The observations show that on graphene the conductivity of nanotube networks is increased by a similar amount as is induced by chemical doping. The Raman spectroscopic measurements, however, reveal no substantial charge transfer between the graphene and nanotube layers. Instead, as probed by temperature dependent conductivity measurements, the graphene support acts as a coupling layer between the individual tubes reducing the tunneling barrier heights. This modification is responsible of enhanced interconnectivity within the binary film that, when used in combination with chemical doping, in our experiments produced sheet resistance as low as $36 \Omega/\square$ at 90% transmittance.

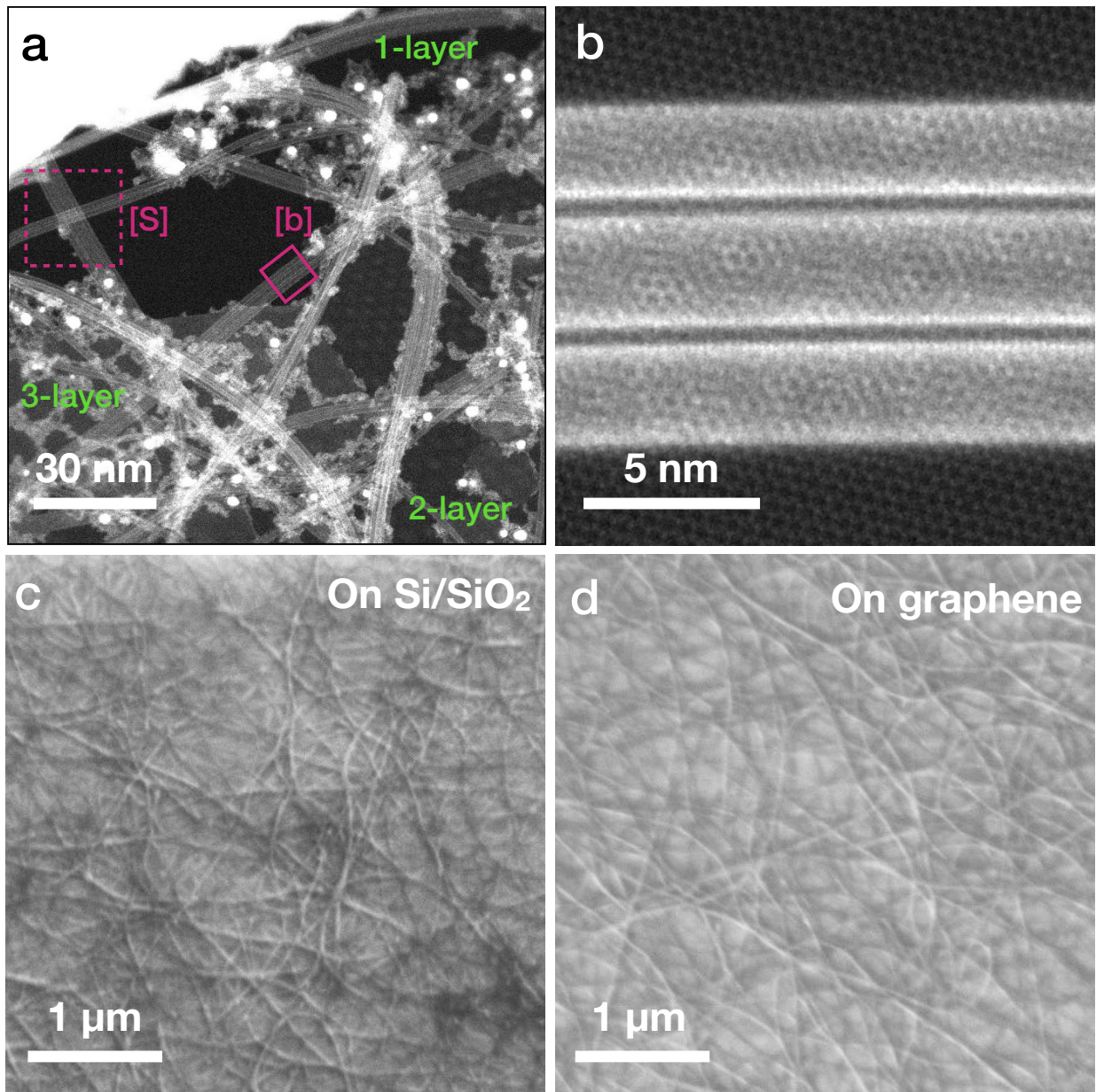


Figure 4: **Thin film morphology** (a) A STEM/MAADF overview of a bundled SWCNT film on graphene. The deposition was carrier out using TP. (b) An atomically resolved close-up of a bundle firmly in contact with graphene. (c) A SEM micrograph of a thermophoretically deposited SWCNT network on SiO₂ and (d) on graphene.

Methods

Thin film fabrication

The SWCNTs were synthesized in a vertical flow floating reactor^{29,30} fed with a total of 400 cm³ min⁻¹ carbon monoxide (CO) and 2 cm³ min⁻¹ of carbon dioxide (CO₂). Of the CO 50

$\text{cm}^3 \text{min}^{-1}$ was additionally passed through a ferrocene cartridge (see FC in Figure 1a) and the mixture passed to the reactor set at 850°C by using a water-cooled injector probe.³⁰ At the tip of the injector SWCNTs were nucleated on the forming iron nanoparticles and grown while traversing through the hot zone. For deposition, we used either a thermophoretic precipitator (TP)³² or vacuum filtration⁴ and quartz windows and silicon dioxide (SiO_2) were used as substrates. The TP consisted of a pair of parallel metal plates kept at ~ 100 K temperature difference and ~ 0.5 mm apart, thus resulting in a $20\,000 \text{ K m}^{-1}$ temperature gradient. This gradient gives rise for thermophoretic force which was then used to drive the floating nanotubes on the substrate placed on the cold surface. The graphene for the experiments was acquired from Graphenea Inc. Finally, the chemical doping was done by dropcasting 16 mM gold chloride solution in acetonitrile on the samples and allowing several minutes of reaction time. Finally, the samples were flushed with pure acetonitrile and left to dry.

Sheet resistance measurements

Sheet resistances were measured by using a Jandel Engineering Ltd. General Purpose 4-point probe system with a RM3000 test unit for resistance readout. The probe head pin layout is a linear array of tungsten needles with a spatial separation of 1 mm.

Spectroscopic measurements

Optical absorption spectra were acquired with an Agilent Cary 5000 spectrophotometer. The samples were supported on 1 mm thick optics grade quartz windows and their contribution was omitted by placing a clean substrate on the reference beamline.

Raman experiments were conducted using a Witech Alpha300 R combined confocal Raman spectroscope and atomic force microscope using 532 nm diode and 633 nm helium-neon laser sources. The nominal power at the sample was set to ~ 0.5 mW with a spot size of ~ 500 nm.

Temperature dependent conductance measurements

These measurements were conducted on networks thermophoretically deposited on square SiO₂ substrates (size 4 mm × 4 mm) with nominal transmittance of ~80% (estimated from the collection time). The four symmetrically placed contact electrodes were fabricated by evaporating gold through a slit mask and manually wire-bonded to a Kyoreca chip carrier.

The measurement apparatus consisted of a liquid helium tank with custom-built vertically movable sample arm including a thermocouple for temperature readout and a Keithley 2635B sourcemeter for 4-point conductivity measurements. Before slowly immersing the sample arm into liquid helium (He), the volume was evacuated to a pressure of 10⁻³ mbar and finally filled with He gas. The cooling rate was kept at ~10 K min⁻¹.

Scanning transmission electron microscopy (STEM)

The electron microscopic imaging was done in an aberration-corrected Nion UltraSTEM 100 operated with a 60-keV primary beam energy, with the sample in ultrahigh vacuum (5 × 10⁻¹⁰ mbar). The angular range for the medium-angle annular dark-field (MAADF) detector was 60–200 mrad. The samples were cleaned with a 6 W continuous wave laser directly attached to the microscope column.⁴⁰

Scanning electron microscopy (SEM)

The images were acquired by using a Zeiss Supra 55 VP analytical SEM with beam energy of 5 kV using the in-lens secondary electron detector.

Acknowledgement

This work was supported by the Academy of Finland *via* projects 286546-DEMEC and 292600-SUPER, by TEKES Finland *via* projects 3303/31/2015 (CNT-PV) and 1882/31/2016 (FEDOC), and the Aalto Energy Efficiency (AEF) Research Program through the MOPPI

project. The authors also thank the funding from the Austrian Science Fund (FWF) under project nos. P 25721-N20, I1283-N20, P 28322-N36 and I3181-N36 and K.M. acknowledges support from the Finnish Foundations' Post Doc Pool. J.K. acknowledges funding from Wiener Wissenschafts- Forschungs- und Technologiefonds through project MA14-009.

Supporting Information Available. STEM images of SWCNT networks on graphene with varying thickness *via* the Internet at <http://pubs.acs.org>.

References

1. Wu, Z.; Chen, Z.; Du, X.; Logan, J. M.; Sippel, J.; Nikolou, M.; Kamaras, K.; Reynolds, J. R.; Tanner, D. B.; Hebard, A. F.; Rinzler, A. G. Transparent, conductive carbon nanotube films. *Science* **2004**, *305*, 1273–1276.
2. Hu, L.; Hecht, D.; Grüner, G. Percolation in transparent and conducting carbon nanotube networks. *Nano letters* **2004**, *4*, 2513–2517.
3. Hecht, D.; Hu, L.; Grüner, G. Conductivity scaling with bundle length and diameter in single walled carbon nanotube networks. *Applied Physics Letters* **2006**, *89*, 133112.
4. Kaskela, A.; Nasibulin, A. G.; Timmermans, M. Y.; Aitchison, B.; Papadimitratos, A.; Tian, Y.; Zhu, Z.; Jiang, H.; Brown, D. P.; Zakhidov, A.; Kauppinen, E. I. Aerosol-synthesized SWCNT networks with tunable conductivity and transparency by a dry transfer technique. *Nano letters* **2010**, *10*, 4349–4355.
5. Hecht, D. S.; Heintz, A. M.; Lee, R.; Hu, L.; Moore, B.; Cucksey, C.; Risser, S. High conductivity transparent carbon nanotube films deposited from superacid. *Nanotechnology* **2011**, *22*, 075201.
6. Mustonen, K.; Susi, T.; Kaskela, A.; Laiho, P.; Tian, Y.; Nasibulin, A. G.; Kauppinen, E. I. Influence of the diameter of single-walled carbon nanotube bundles on the

- optoelectronic performance of dry-deposited thin films. *Beilstein journal of nanotechnology* **2012**, *3*, 692.
7. Mustonen, K.; Laiho, P.; Kaskela, A.; Zhu, Z.; Reynaud, O.; Houbenov, N.; Tian, Y.; Susi, T.; Jiang, H.; Nasibulin, A. G.; Kauppinen, E. I. Gas phase synthesis of non-bundled, small diameter single-walled carbon nanotubes with near-armchair chiralities. *Applied Physics Letters* **2015**, *107*, 013106.
 8. Mustonen, K.; Laiho, P.; Kaskela, A.; Susi, T.; Nasibulin, A. G.; Kauppinen, E. I. Uncovering the ultimate performance of single-walled carbon nanotube films as transparent conductors. *Applied Physics Letters* **2015**, *107*, 143113.
 9. Jiang, S.; Hou, P.-X.; Chen, M.-L.; Wang, B.-W.; Sun, D.-M.; Tang, D.-M.; Jin, Q.; Guo, Q.-X.; Zhang, D.-D.; Du, J.-H.; Tai, K.-P.; Tan, J.; Kauppinen, E. I.; Liu, C.; Cheng, H.-M. Ultrahigh-performance transparent conductive films of carbon-welded isolated single-wall carbon nanotubes. *Science advances* **2018**, *4*, eaap9264.
 10. Lee, R.; Kim, H.; Fischer, J.; Thess, A.; Smalley, R. E. Conductivity enhancement in single-walled carbon nanotube bundles doped with K and Br. *Nature* **1997**, *388*, 255.
 11. Choi, H. C.; Shim, M.; Bangsaruntip, S.; Dai, H. Spontaneous reduction of metal ions on the sidewalls of carbon nanotubes. *Journal of the American Chemical Society* **2002**, *124*, 9058–9059.
 12. Kim, K. K.; Bae, J. J.; Park, H. K.; Kim, S. M.; Geng, H.-Z.; Park, K. A.; Shin, H.-J.; Yoon, S.-M.; Benayad, A.; Choi, J.-Y.; Lee, Y. H. Fermi level engineering of single-walled carbon nanotubes by AuCl₃ doping. *Journal of the American Chemical Society* **2008**, *130*, 12757–12761.
 13. Fuhrer, M.; Nygård, J.; Shih, L.; Forero, M.; Yoon, Y.-G.; Choi, H. J.; Ihm, J.; Louie, S. G.; Zettl, A.; McEuen, P. L. Crossed nanotube junctions. *Science* **2000**, *288*, 494–497.

14. Nirmalraj, P. N.; Lyons, P. E.; De, S.; Coleman, J. N.; Boland, J. J. Electrical connectivity in single-walled carbon nanotube networks. *Nano letters* **2009**, *9*, 3890–3895.
15. Znidarsic, A.; Kaskela, A.; Laiho, P.; Gaberscek, M.; Ohno, Y.; Nasibulin, A. G.; Kauppinen, E. I.; Hassanien, A. Spatially resolved transport properties of pristine and doped single-walled carbon nanotube networks. *The Journal of Physical Chemistry C* **2013**, *117*, 13324–13330.
16. Chen, M.; Li, W.; da Silveira Venzel, T. E.; Li, G.; Itkis, M. E.; Haddon, R. C.; Bekyarova, E. Effect of constructive rehybridization on transverse conductivity of aligned single-walled carbon nanotube films. *Materials Today* **2018**, *21*, 937–943.
17. Pereira, L. F.; Rocha, C.; Latgé, A.; Coleman, J.; Ferreira, M. Upper bound for the conductivity of nanotube networks. *Applied Physics Letters* **2009**, *95*, 123106.
18. Tung, V. C.; Chen, L.-M.; Allen, M. J.; Wassei, J. K.; Nelson, K.; Kaner, R. B.; Yang, Y. Low-temperature solution processing of graphene- carbon nanotube hybrid materials for high-performance transparent conductors. *Nano letters* **2009**, *9*, 1949–1955.
19. Gorkina, A. L.; Tsapenko, A. P.; Gilshteyn, E. P.; Koltsova, T. S.; Larionova, T. V.; Talyzin, A.; Anisimov, A. S.; Anoshkin, I. V.; Kauppinen, E. I.; Tolochko, O. V.; Nasibulin, A. G. Transparent and conductive hybrid graphene/carbon nanotube films. *Carbon* **2016**, *100*, 501–507.
20. Bittolo Bon, S.; Valentini, L.; Kenny, J.; Peponi, L.; Verdejo, R.; Lopez-Manchado, M. Electrodeposition of transparent and conducting graphene/carbon nanotube thin films. *physica status solidi (a)* **2010**, *207*, 2461–2466.
21. Hong, T.-K.; Lee, D. W.; Choi, H. J.; Shin, H. S.; Kim, B.-S. Transparent, flexible conducting hybrid multilayer thin films of multiwalled carbon nanotubes with graphene nanosheets. *Acs Nano* **2010**, *4*, 3861–3868.

22. Kholmanov, I. N.; Magnuson, C. W.; Piner, R.; Kim, J.-Y.; Aliev, A. E.; Tan, C.; Kim, T. Y.; Zakhidov, A. A.; Sberveglieri, G.; Baughman, R. H.; Ruoff, R. S. Optical, electrical, and electromechanical properties of hybrid graphene/carbon nanotube films. *Advanced Materials* **2015**, *27*, 3053–3059.
23. Kim, Y.-K.; Min, D.-H. Durable large-area thin films of graphene/carbon nanotube double layers as a transparent electrode. *Langmuir* **2009**, *25*, 11302–11306.
24. Li, C.; Li, Z.; Zhu, H.; Wang, K.; Wei, J.; Li, X.; Sun, P.; Zhang, H.; Wu, D. Graphene nano-“patches” on a carbon nanotube network for highly transparent/conductive thin film applications. *The Journal of Physical Chemistry C* **2010**, *114*, 14008–14012.
25. Liu, Y.-T.; Feng, Q.-P.; Xie, X.-M.; Ye, X.-Y. The production of flexible and transparent conductive films of carbon nanotube/graphene networks coordinated by divalent metal (Cu, Ca or Mg) ions. *Carbon* **2011**, *49*, 3371–3375.
26. Nguyen, D. D.; Tai, N.-H.; Chen, S.-Y.; Chueh, Y.-L. Controlled growth of carbon nanotube–graphene hybrid materials for flexible and transparent conductors and electron field emitters. *Nanoscale* **2012**, *4*, 632–638.
27. Yang, T.; Yang, J.; Shi, L.; Mäder, E.; Zheng, Q. Highly flexible transparent conductive graphene/single-walled carbon nanotube nanocomposite films produced by Langmuir–Blodgett assembly. *RSC Advances* **2015**, *5*, 23650–23657.
28. Nasibulin, A. G.; Kaskela, A.; Mustonen, K.; Anisimov, A. S.; Ruiz, V.; Kivisto, S.; Rackauskas, S.; Timmermans, M. Y.; Pudas, M.; Aitchison, B.; Kauppinen, M.; Brown, D. P.; Okhotnikov, O. G.; Kauppinen, E. I. Multifunctional free-standing single-walled carbon nanotube films. *ACS nano* **2011**, *5*, 3214–3221.
29. Liao, Y.; Jiang, H.; Wei, N.; Laiho, P.; Zhang, Q.; Khan, S. A.; Kauppinen, E. I. Direct Synthesis of Colorful Single-Walled Carbon Nanotube Thin Films. *Journal of the American Chemical Society* **2018**, *140*, 9797–9800.

30. Moisala, A.; Nasibulin, A. G.; Brown, D. P.; Jiang, H.; Khriachtchev, L.; Kauppinen, E. I. Single-walled carbon nanotube synthesis using ferrocene and iron pentacarbonyl in a laminar flow reactor. *Chemical Engineering Science* **2006**, *61*, 4393–4402.
31. Liao, Y.; Hussain, A.; Laiho, P.; Zhang, Q.; Tian, Y.; Wei, N.; Ding, E.-X.; Khan, S. A.; Nguyen, N. N.; Ahmad, S.; Kauppinen, E. I. Tuning Geometry of SWCNTs by CO₂ in Floating Catalyst CVD for High-Performance Transparent Conductive Films. *Advanced Materials Interfaces* **2018**, *5*, 1801209.
32. Laiho, P.; Mustonen, K.; Ohno, Y.; Maruyama, S.; Kauppinen, E. I. Dry and direct deposition of aerosol-synthesized single-walled carbon nanotubes by thermophoresis. *ACS applied materials & interfaces* **2017**, *9*, 20738–20747.
33. Pike, G.; Seager, C. Percolation and conductivity: A computer study. I. *Physical review B* **1974**, *10*, 1421.
34. Bae, S.; Kim, H.; Lee, Y.; Xu, X.; Park, J.-S.; Zheng, Y.; Balakrishnan, J.; Lei, T.; Kim, H. R.; Song, Y. I.; Kim, Y.-J.; Kim, K. S.; Özyilmaz, B.; Ahn, J.-H.; Hong, B. H.; Iijima, S. Roll-to-roll production of 30-inch graphene films for transparent electrodes. *Nature nanotechnology* **2010**, *5*, 574.
35. Sheng, P. Fluctuation-induced tunneling conduction in disordered materials. *Physical Review B* **1980**, *21*, 2180.
36. Pietronero, L. Ideal conductivity of carbon π polymers and intercalation compounds. *Synthetic Metals* **1983**, *8*, 225–231.
37. Kaiser, A. B. Electronic transport properties of conducting polymers and carbon nanotubes. *Reports on Progress in Physics* **2001**, *64*, 1.
38. Wang, F.; Sfeir, M. Y.; Huang, L.; Huang, X. H.; Wu, Y.; Kim, J.; Hone, J.; O'Brien, S.;

- Brus, L. E.; Heinz, T. F. Interactions between individual carbon nanotubes studied by Rayleigh scattering spectroscopy. *Physical review letters* **2006**, *96*, 167401.
39. Mustonen, K.; Hussain, A.; Hofer, C.; Monazam, M. R.; Mirzayev, R.; Elibol, K.; Laiho, P.; Mangler, C.; Jiang, H.; Susi, T.; Kauppinen, E. I.; Kotakoski, J.; Meyer, J. C. Atomic-Scale Deformations at the Interface of a Mixed-Dimensional van der Waals Heterostructure. *ACS nano* **2018**, *12*, 8512–8519.
40. Tripathi, M.; Mittelberger, A.; Mustonen, K.; Mangler, C.; Kotakoski, J.; Meyer, J. C.; Susi, T. Cleaning graphene: Comparing heat treatments in air and in vacuum. *physica status solidi (RRL)–Rapid Research Letters* **2017**, *11*, 1700124.
41. Liew, K.; Wong, C.; Tan, M. Buckling properties of carbon nanotube bundles. *Applied Physics Letters* **2005**, *87*, 041901.
42. Paulson, S.; Helser, A.; Nardelli, M. B.; Taylor, R.; Falvo, M.; Superfine, R.; Washburn, S. Tunable Resistance of a Carbon Nanotube-Graphite Interface. *Science* **2000**, *290*, 1742–1744.
43. Homma, Y.; Suzuki, S.; Kobayashi, Y.; Nagase, M.; Takagi, D. Mechanism of bright selective imaging of single-walled carbon nanotubes on insulators by scanning electron microscopy. *Applied Physics Letters* **2004**, *84*, 1750–1752.
44. Loos, J.; Alexeev, A.; Grossiord, N.; Koning, C. E.; Regev, O. Visualization of single-wall carbon nanotube (SWNT) networks in conductive polystyrene nanocomposites by charge contrast imaging. *Ultramicroscopy* **2005**, *104*, 160–167.
45. Sun, D.-M.; Timmermans, M. Y.; Tian, Y.; Nasibulin, A. G.; Kauppinen, E. I.; Kishimoto, S.; Mizutani, T.; Ohno, Y. Flexible high-performance carbon nanotube integrated circuits. *Nature nanotechnology* **2011**, *6*, 156.

Supporting Information

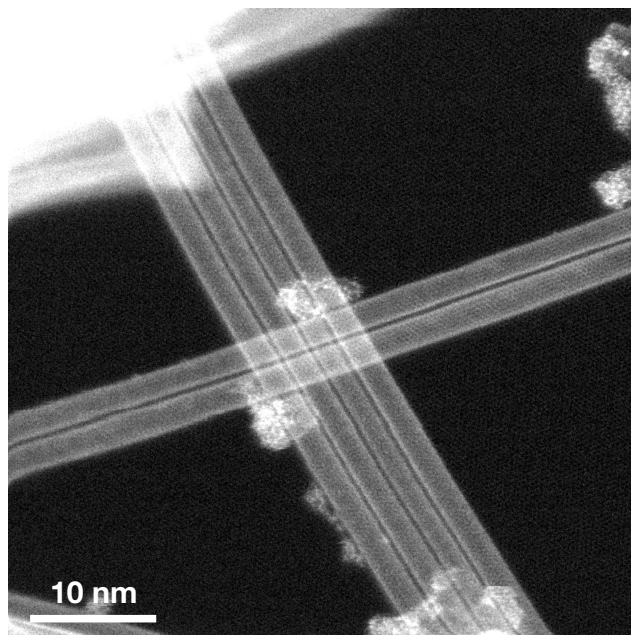


Figure S1: STEM/MAADF closeup of two bundles forming an X-junction in Figure 2.

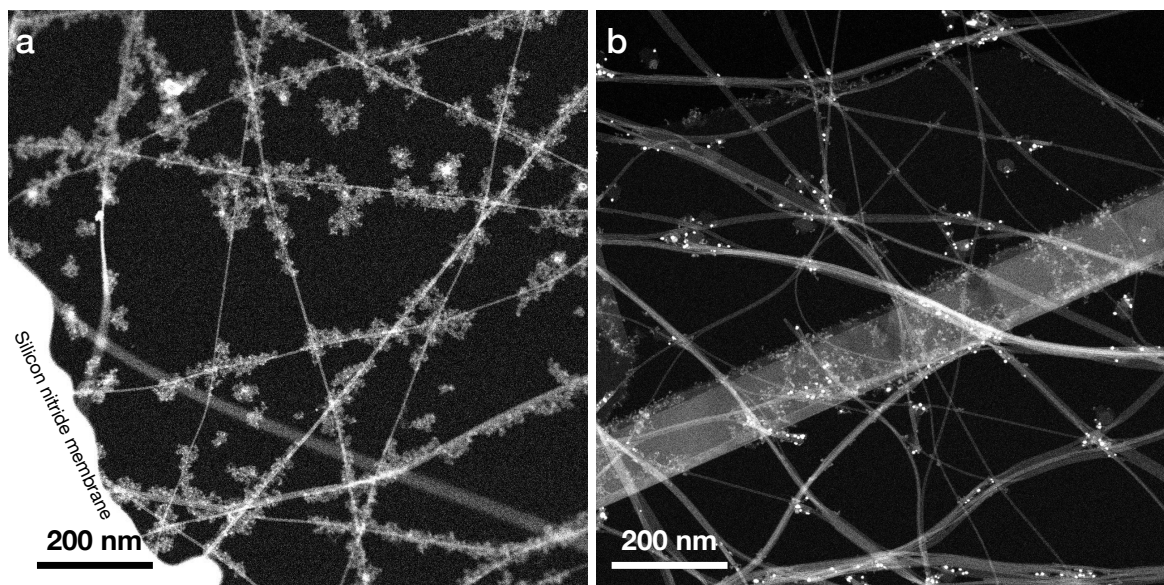


Figure S2: STEM/MAADF images of different SWCNT layer thicknesses on laser cleaned graphene.⁴⁰ Note how the morphology qualitatively changes from one dominated by X-junctions to Y-junctions when the deposition time is increases from 2 minutes in (a) to 10 minutes in (b).